Things Measured by Cone Penetration Tests other than Material Properties

Tadashi KAWAI
Associate professor, Civil and Environmental Engineering, Tohoku University, Sendai, Japan
Email: tadashi.kawai.b2@tohoku.ac.jp
Kotaro KUBOTA
Former Graduate Student, Civil and Environmental Engineering, Tohoku University, Sendai, Japan
Jong-Kwan KIM
Researcher, Geotech. Eng. Research Inst., Korea Inst. of Civil Eng. and Building Tech., Goyang, Korea
Motoki KAZAMA
Professor, Civil and Environmental Engineering, Tohoku University, Sendai, Japan
Toshihiro NODA
Professor, Disaster Mitigation Research Center, Nagoya University, Nagoya, Japan

ABSTRACT

The cone penetration test is a proven method for evaluating soil properties, yet relatively little research has been conducted to understand penetrometer readings (CPT-data) as a complicated boundary value problem. The interpretation of CPT-data tends to rely on empirical relationships, many of which have been developed over the years for soil identification and classification. Those studies tend to have an implicit expectation that the relationship between the CPT-data and a single soil parameter is independent, e.g. the friction angle can be estimated directly from CPT-data without the need to consider any boundary value problems. In this study, a series of numerical analysis by using FEM (GEOASIA) was conducted to demonstrate the complexity of the penetration mechanism. A description of the calculation procedures is first provided with some preliminary calculation results with various displacement ratios at the supposed cone apex. The results highlight the differences in the resistances at the cone tip even when the friction angle is the same and are evidence of the complexity of the penetration problem.

Key words: *Cone penetration, Stratigraphic order, FEM, Deformation*

1. Introduction

The Cone Penetration Test (CPT) is extensively used as an in-situ soil investigation method. The estimation of soil parameters, such as the internal friction angle, are typically performed using the cone penetration resistance obtained from the CPT. However, since cone penetration resistance is not a physical parameter unique to soil material but rather a response value of the ground, it is reasonable to assume that estimating soil parameters directly from cone penetration resistance is problematic, at best. Even though the cone penetration test is a proven method for evaluating soil properties, relatively little research has been conducted to understand penetrometer readings as a complicated boundary value problem.

One of a complicating factors in the interpretation of CPT data is that readings are influenced not only by the soil at the location of the cone tip but also by the soil within an influence zone which extends some distance both beneath and above the tip. Ahmadi & Robertson (2005) studied the 'thin-layer effects' on the CPT-data. They conducted a series of FEM numerical analyses using so-called cavity expansion modeling and concluded that the full tip resistance may not be reached in thin stiff layers because of the influence of the upper/lower softer layers. Recently, Mo *et al*. (2017) also conducted the similar systematic analysis and compared their numerical results

with the field data. Further, Ma *et al*. (2017) conducted an extensive parametric study using a large deformation finite-element analyses, then, based on their numerical results, they proposed a procedure for interpreting the layer boundaries and undrained shear strength from measured CPT-data after taking the thin-layer effect into account. Meanwhile, an experimental investigation by Mo *et al*. (2015) obtained the extent of soil deformation around a penetrated cone using centrifuge testing. Their results revealed that the cone penetration is a complicated boundary value problem. As for the field CPT-data, Thevanayagam *et al*. (2017) evaluated the relationships between liquefaction resistance and CPT-data and considered the combined effect of penetration velocity and the coefficient of consolidation $C_{v,}$ which is composed of permeability k and compressibility m_v. This can be considered field evidence that the cone penetration is a complicated boundary value problem. Therefore, in order to obtain the soil properties of the target location, the response behavior of the soil should be evaluated as a boundary value problems which takes the many factors shown in **Fig. 1** into account at the same time: consolidation (drainage), shear deformation and the dilatancy of the target soil and its neighbor layers.

As preparation for a future numerical investigation focused on the details of the combined effects of soil properties and various boundary conditions, a series of numerical analyses was conducted using a FEM code named GEOASIA® (All Soils All States All Round Geo-analysis Integration) developed by Asaoka *et al*. (1998a), Asaoka & Noda (2007) and sophisticated by Noda *et al*. (2008), in which the Super/subloading Yield Surface Cam-clay model, in short, the SYS Cam-clay model (Asaoka . 1998b, 2000, 2002) was used as the constitutive equation of the soil skeleton. As shown in the results reported by Tolooiyan & Gavin (2011) from a series of numerical simulations using multiple soil modeling methods and obtained different results, the soil modeling methods greatly influence the obtained results. As such, in order to evaluate the complicated boundary value problem, it is clearly necessary to adopt a more sophisticated model which represents soil behavior as close to reality as possible.

Among the various analysis methods of cone resistance, Mo . (2017) adopted the so-called cavity expansion modeling to realize the soil responses during cone penetration after careful consideration of the experimental results. The validity of the modeling method was also carefully confirmed by Ahmadi . (2005) and Ahmadi & Dariani (2017). Therefore, the same modeling method was adopted in this study. A description of the calculation procedures is firstly provided with some preliminary calculation results achieved by the use of various displacement ratios at the supposed cone apex and the upper rod.

There has been relatively little research done on the effect of soil dilatancy on CPT measurements related to layered configurations. Neither the detailed soil stress-strain and dilatancy-strain histories associated with CPT nor the relationship to the distribution of the load on the probe are well understood. Therefore, the results which show different cone tip resistances despite the same friction angle are then provided to highlight complexity of the penetration problem.

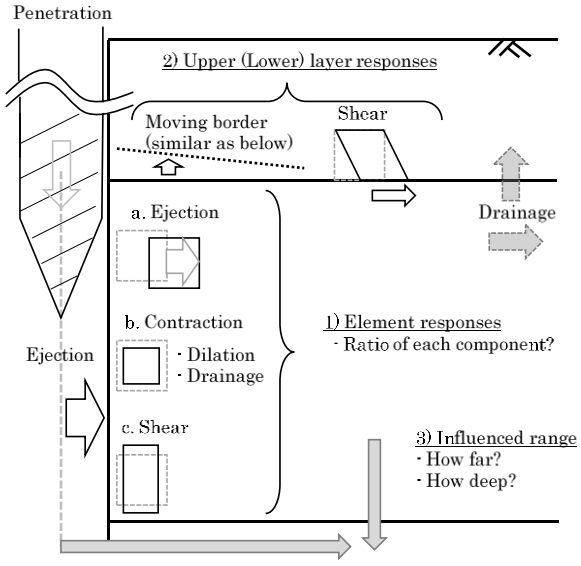

Fig. 1 Penetration mechanisms; the logic solving it as a boundary value problem

2. Numerical analysis - Models and settings

The finite element mesh and boundary conditions used are shown in **Fig. 2**. The over burden pressure equivalent to the depth of 9.0 m with the same density as Layer 1 is given at the top of the model. The effect of the gravity force was taken into account in the calculations. The penetration part is magnified in **Fig. 3**, where the

axisymmetric coordinates were adopted. As shown in **Fig. 3**, the nodal points on the left-hand side border of the FEM mesh, which were pushed away toward the right-hand side and downward along the supposed cone path, were directly moved to realize the ground movements during cone penetration by following the cavity expansion modeling described in Armadi & Robertson (2005) in detail. The nodal points were moved from the top one. The supposed cone apex angle and diameter were 60 degrees and 30 mm respectively, then the horizontal displacement of each nodal point was as much as 15 mm after all four calculation stages; each calculation stage involved 2500 time integration steps (time span 0.0005 s) at a cone penetration speed of about 5 mm/s toward the depth. These size and speed parameters were set as a preliminary study for future experimental validations by using a calibration chamber and a miniature cone.

The required material constants and the meanings of each parameter are listed in **Table 1**. The parameter values set for virtual models used in this study are given in **Table 2** along with the initial values (**Table 3**) describing the initial soil state. These values are expected to provide a vague image of loose and dense sand for Layer 1 and Layer 2 (2-1, 2-2, 2-3), respectively. All of the shear modulus and strength settings of Layer 2 series were given for a common dense sand image, but different dilatancy characteristics were used. One of the strong points of numerical investigation is that the soil behaviors can be easily changed in order to study the influences from each of soil characteristic separately. **Fig. 4** shows the element behaviors (drained triaxial loading) using the SYS Cam-clay model for the material parameter sets of 2-1, 2-2, 2-3.

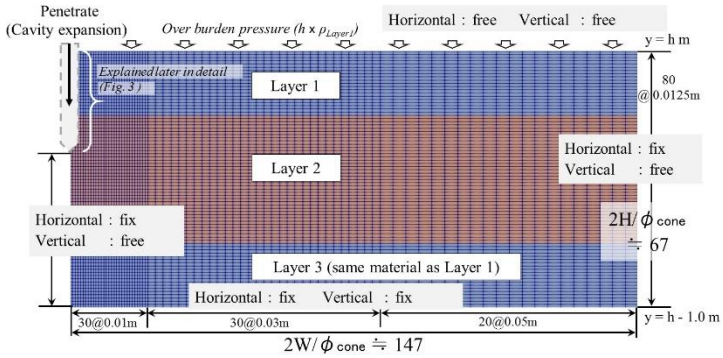

Fig. 2 axisymmetric FEM mesh and boundary conditions

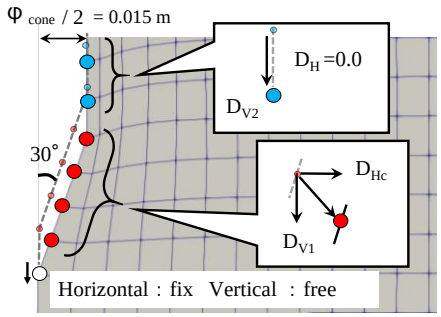

Fig. 3 Calculated procedures of cone penetration

Table 1. Meanings of each material property in SYS Cam-clay model

A. Elasto-plastic parameters
A1: Compression index $\tilde{\lambda}$
A2: Swelling index $\tilde{\kappa}$
A3: Critical state constant M
A4: Specific volume at q=0 and p'=98.1 (kPa) on NCL N
A5: Poisson's ratio ν
B. Evolution rule parameters
B1: Degradation index of structure a (b =c =1.0)
B2: Degradation index of overconsolidation m
B3: Evolution index of rotational hardening b_r
B4: Limit of rotational hardening m_b
C. Permeability k (cm/s)
D. Specific gravity of soil particles G_s

Table 2. Settings of the material parameters for each layer

	Layer 1 (loose)	Layer 2 2-1	2-2	2-3
A1: λ	0.046	0.060	0.080	0.100
A2: κ	0.0055	0.0080	0.0026	0.0040
A3: M	1.40	1.35	1.35	1.08
A4: N	1.73	1.90	1.99	2.06
A5: ν	0.3	0.3	0.3	0.3
B1: a	0.73	5.00	4.00	5.00
B2: m	0.30	0.09	0.21	0.13
B3: b_r	0.5	2.5	1.0	5.0
B4: m_b	0.5	0.8	0.7	1.0
C: k	0.001	0.010	0.010	0.010
D: G_s	2.65	2.65	2.65	2.65

Table 3. Settings of the initial conditions for each layer

	Layer 1 (loose)	Layer 2 2-1	2-2	2-3
Degree of overconsolidation 1/R	2	142	152	363
Degree of structure 1/R*	25	1.5	1.5	2
Lateral stress ratio	1.0	0.6	0.6	0.6
Specific volume v0	1.80	1.82	1.84	1.82

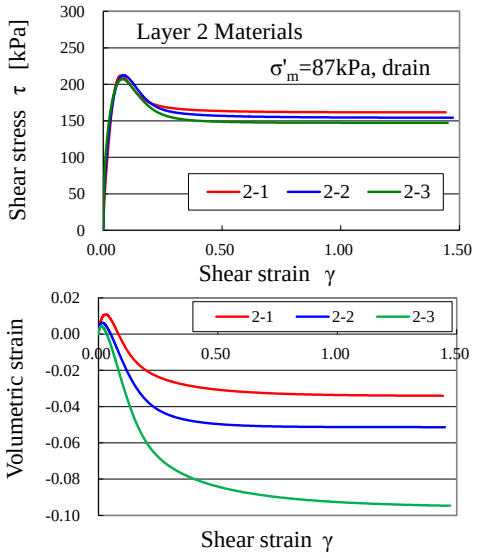

Fig. 4 Examples of the element responses of SYS Cam clay model calculated by using the material properties shown in Table 2 and 3.

3. Numerical analysis - Preliminary calculations

Since the functions to define friction are limited at the border, i.e. FEM mesh boundary or the contact surface between two different materials, they are not implemented in the FEM code used in this study, and the magnitudes of the vertical displacements at the cone apex and rod must be prescribed. As the numerically achieved results of Ahmadi . (2005) and also the experimentally achieved results of Arshad . (2014) show, since the ratio of vertical displacement to horizontal displacement is dependent on the various conditions, e.g. material kinds, penetration speed, and so on, there is no hint to determine the value of the ratio without an concrete target image. In abandoning any attempt to validate the value adopted in this study, our focus was on investigating the dilatancy effect on the penetration resistances by calculating a virtual soil model: a series of numerical analyses were conducted to grasp the extent of influence of the displacement ratios on the penetration resistance, as shown in **Table 4**.

Before comparing those results, in order to help develop a realistic image of the soil behavior caused by penetration, various contours for Case 1, which is the standard case in this study, were prepared, as seen **Fig. 5**. In this figure, the same components of stress are arranged in the same column and the results at the same penetration depth are arranged in the same row. In each contour, two dotted lines are drawn to make it easy to see the borders between Layer 1 (loose; contractive) and Layer 2 (dense; expansive), and also Layer 2 and Layer 3 (loose; contractive). The ranges of all the stress contours were unified from -30 kPa to 30 kPa. By the penetration, the vertical stress mainly increases downward positively, which is translated as compression in this figure, and the horizontal stress tends to increase laterally at first. This lateral compression moves not only the lateral soil surrounding the CPT-rod but also the soil located below the penetration depth, as such the lateral stress directly beneath the cone center is slightly reduced as a consequence. If the soil moves outside toward the radius direction, the larger r results in a larger volume, and this results in a reduction in the circumferential stress component.

The volumetric strain contours are also shown in **Fig. 5**. In spite of the high lateral compression along the CPT-rod, all the highly sheared elements in the two or three lines from the penetration border showed expansion, even in Layer 1, which was composed of the contractive loose sand. Then, outside of those elements, a highly contracted area suddenly emerged especially in Layer 1. This contracted zone was attenuated gradually toward the outside. While all these soil behaviors seem rational, they suggest that penetration is a complex problem of soil deformation. Further, because of the existence of the layer boundaries, the stress distributions indicates considerable complexity in the penetration mechanisms.

Table 4. Cases for searching the appropriate vertical displacement ratios

#	R_1 (D_{V1}/D_{Hc})	R_2 (D_{V2}/D_{V1})	Layer 2
Case1	0.5	0.08	2-1
Case2-1	0.9		
Case2-2	0.7		
Case2-3	0.3	0.08	2-1
Case2-4	0.1		
Case2-5	0		
Case3-1		0.12	
Case3-2	0.5	0.05	2-1
Case3-3		0.03	

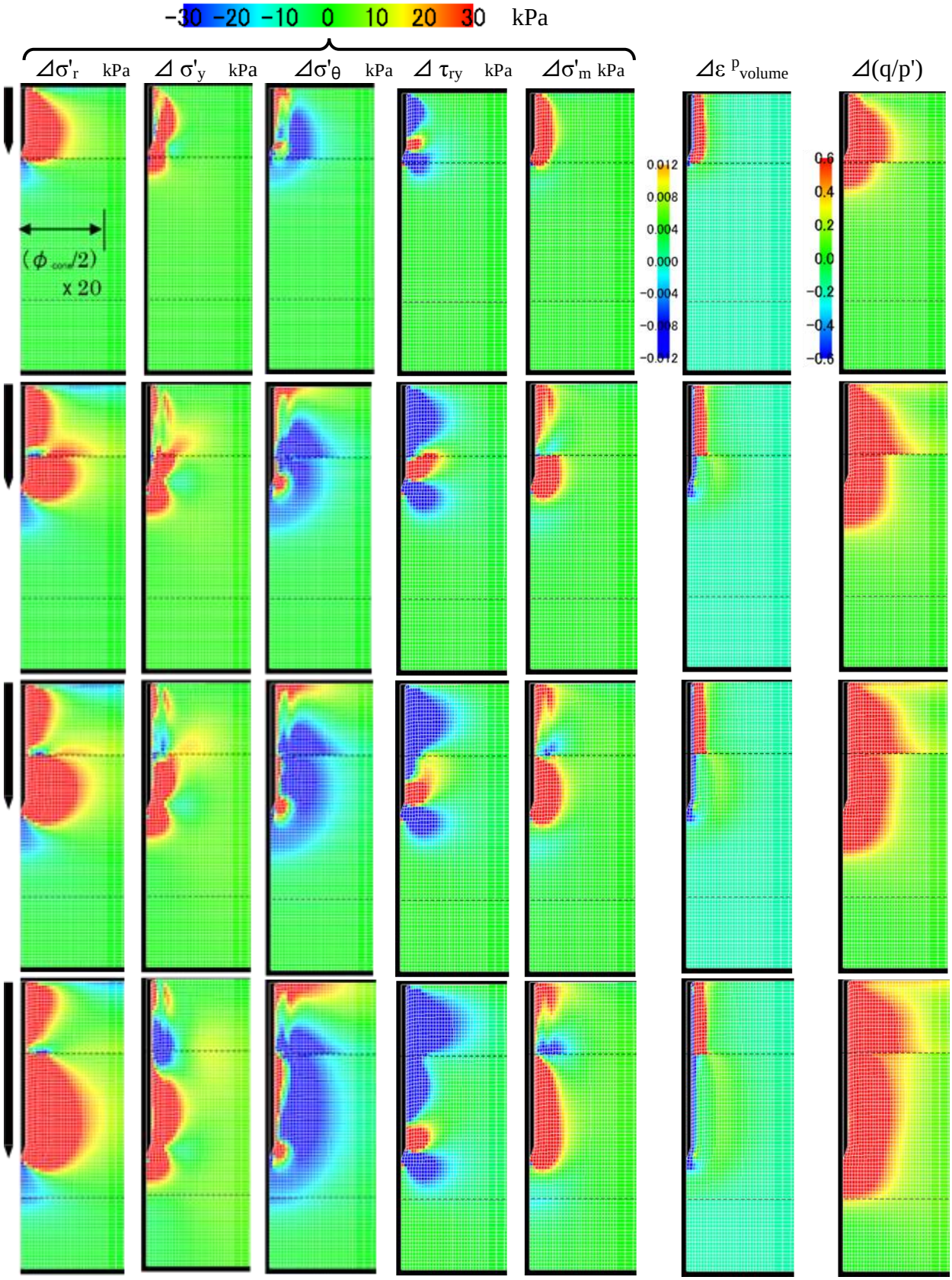

Fig. 5 Typical penetration influence on the increments of stress components and volumetric strain (Case1).

In order to simulate the deformation of soils around the cone tip by penetration, it is necessary to apply horizontal displacement and vertical displacement to the nodal points where the cone tip penetration is realized, and to apply vertical displacement to the nodal points to represent the rod after passing through the cone tip. Although the final horizontal displacement obviously becomes equal to that of the cone radius, the extent of the vertical displacement is unclear, and is dependent on the various conditions cited by Ahmadi . (2005).

In order to grasp the extent of influence of the displacement ratios on the penetration resistance, a series of analyses was carried out in which the ratio (R_1) of the vertical displacement to the horizontal displacement at the cone apex was changed to 0, 0.1, 0.3, 0.5, 0.7, 0.9. The tip resistances of those analyses are plotted in **Fig. 6**; the lateral and vertical axes are tip resistance and depth, respectively. The cone tip resistance for each value of penetration was calculated from the summation of the contributions of the related elements which configure the cone tip apex. That is, the vertical pressure and the vertical component of shear stress were multiplied by the side area of each element.

As reported by Ahmadi . (2005), it was confirmed that with increasing vertical displacement at the cone apex, the tip resistance becomes larger, as shown in **Fig. 6**. Further, with increases in the vertical displacement ratio, the range of the influenced zone becomes larger, as shown in **Fig. 7**. As mentioned above, because no value for the vertical displacement ratio was considered correct in this study, a value of 0.5 was adopted in the later analyses for convenience. It is noted that this is smaller than the realistic number confirmed by Ahmadi . (2005) in their comparison of the calculated results with experimental measurements. This smaller value is expected to result in a shallower zone of influence below the cone tip.

In cone penetration, because the soil around the rod is continuously dragged vertically downward by sleeve friction during penetration, vertical displacement occurs. As yet, however, no detailed investigation has been carried out to determine how much displacement occurs. Therefore, by applying the vertical displacement to the nodes at the rod after passing through the cone tip, the drag due to sleeve friction was reproduced and its influence was investigated. The ratios (R_2) of the vertical displacement at the rod to the one at the cone apex were set 0.12, 0.08, 0.05, or 0.03. Contrary to the apparent influences of the vertical displacement ratio at the cone apex, around the cone shaft the vertical displacement ratio had little effect on the penetration resistance, as shown in **Fig. 8**. A ratio of 0.08 was therefore adopted: there was no specific motivation in choosing this value.

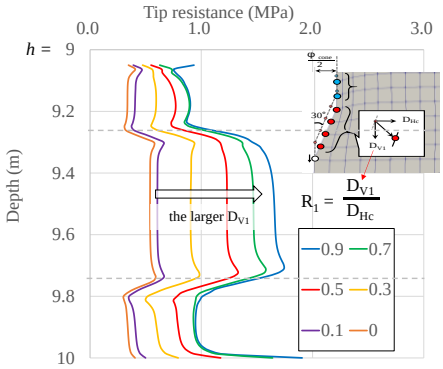

Fig. 6 Influence of the vertical displacement ratio at the cone apex on the tip resistance

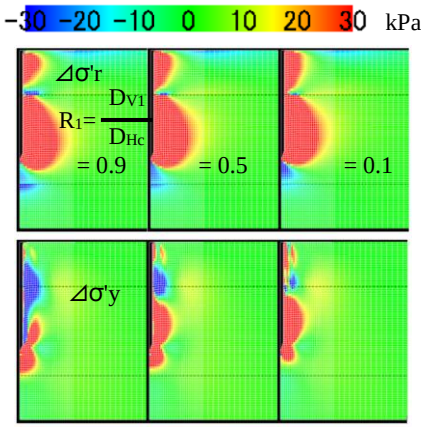

Fig. 7 Stress distributions around and beneath the penetrated cone.

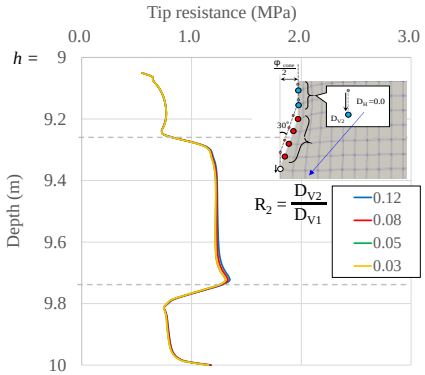

Fig. 8 Influence of the vertical displacement ratio around the cone shaft on the tip resistance

4. Numerical analysis - Influence of soil dilatancy

In order to confirm that the cone penetration is indeed the complicated problem suggested by **Fig. 1**, a series of calculations was carried out using soil materials having the same shear stress-shear strain relation but different dilatancies (**Table 5**). The complicated nature of the problem is thought to be related to the volumetric balance of the space, which is an equilibrium of conservation of mass caused by elastic volume change, consolidation, dilatancy and ejections. Because it is implicitly expected that there should be a unique relationship in the empirical co-relations between the cone tip resistances and the friction angles of sandy soils, the results is useful to estimate the in-situ friction angles from the cone tip resistance. If it were valid, since the shear stress-shear strain relation is similar, as confirmed in **Fig. 4**, which means the internal friction angle is equal, the measured tip resistances would be also similar. However, despite having the same strength, there is a large difference in the tip resistances, as shown in **Fig. 9**. On the other hand, the tip resistances from Case4-1 (Mat. #2-2) and Case4-2 (Mat. #2-3) were almost the same in spite of their different dilatancy. The stress and volumetric strain distributions shown in **Figs. 10** and **11** were taken into account to develop a possible reason for this, as explained below.

Fig. 10 shows the vertical stress distributions at the two stages of penetration: the contour ranges of these cases was adjusted to be more sensitive than those in **Fig. 5**. Although the stress increasing range did not extend to the border between Layer 2 and Layer 3 in Case 1 (material #2-1) in the earlier stage shown in upper row in **Fig. 10**, those ranges in the other two cases had already reached to the border. Therefore, a comparison of the tip resistances in **Fig. 9** indicates that until this stage of penetration, the resistance was larger with larger dilatancies. On the other hand, after this penetration stage, since the material properties and/or responses of Layer 3 might be reflected in the tip resistance at Layer 2 only in Case 4-1 and 4-2, the tip resistances of those two cases became asymptotically the same value despite the differences in dilatancy. It should be acknowledged that the change in the contour range gives different impressions depending on the maximum value, and there does not appear to be any logical meaning in adopting the value of 6 kPa, as we did. However, the sudden increase of the tip resistance of Case 1 in Layer 2 at the later stage of penetration, where the cone tip comes closer to Layer 3 (loose) and the resistance is expected to decrease, suggests that adopting 0.6 as the value had meaning. This is because the stress increasing zone recognized by the contour reached the bottom boundary in Case 1 at the point which corresponds to the sudden increase of the tip resistance shown in **Fig. 9**. That is, the cone tip sensed the bottom boundary through Layer 3 as it penetrated Layer 2.

Table 5. Trial cases to grasp dilatancy effects

#	R_1 (D_{V1}/D_{Hc})	R_2 (D_{V2}/D_{V1})	Layer 2
Case1	0.5	0.08	2-1
Case4-1	0.5	0.08	2-2
Case4-2			2-3

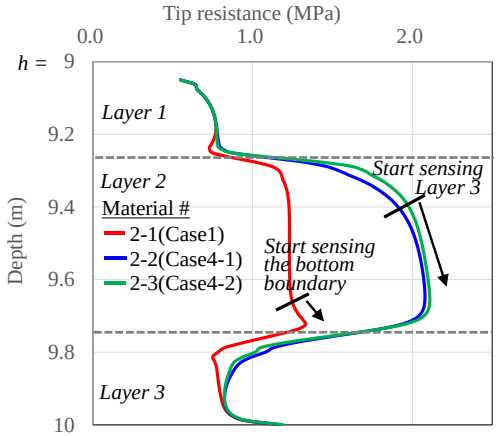

Fig. 9 Influence of the dilatancy characteristics of the Layer 2 material and the stratigraphy on the tip resistance

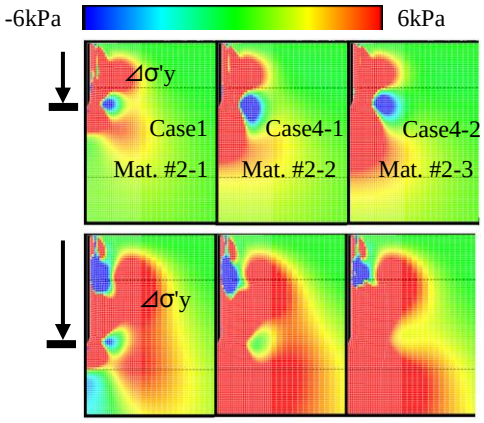

Fig. 10 Vertical stress distributions at the two stages of penetration process; the stress increased zone reached the boundary between Layer 2 and Layer 3 in Case 4-1 and 4-2 (upper), the stress increased zone reached the bottom boundary in Case 1 (lower)

5. Concluding remarks

As preparation for a future numerical investigation on the details of the combined effects of soil properties and various boundary conditions on cone penetration resistance, a series of numerical analysis was conducted using a FEM code named GEOASIA. After a preliminary study designed to reveal the vertical displacements around the cone apex and rod, a value of 0.5 times of the horizontal displacement was adopted for the vertical displacement at the cone apex, which was less than the result reported in the literature from experimental studies. Although the vertical displacement adopted was moderate and was expected to result in a smaller influence zone than that in a case with larger vertical displacement like the experimental value, the cone tip resistances were sensitive to the combined effects between the boundary conditions and the deformation characteristics. This was especially the case with regard to the dilatancy of soils.

The authors freely acknowledge that besides being conducted in-situ, this study was employed slightly exaggerated conditions both with regard to the material properties and the boundary conditions. As such, further investigations are needed to prove the validity of the modeling method. A comparison of a series of calibration chamber tests, and then a series of numerical parametric studies based on proper analytical conditions is required in order to determine the precise nature of those combined effects in practice.

References

Ahmadi, M. M., Byrne, P. M. & Campanella, R. G. 2005. Cone tip resistance in sand: modeling, verification, and applications. Canadian Geotech. J. , 42 (4) , pp. 977-993.

Ahmadi, M. M. & Robertson, P. K. 2005. Thin-layer effects on the CPT qc measurement. Canadian Geotech. J. , 42 (5) , pp. 1302-1317.

Ahmadi, M.M. & Dariani Golestani, A.A. 2017. Cone penetration test in sand: A numerical-analytical approach. Computers and Geotechnics, 90, pp. 176-189.

Arshad, M.I., Tehrani, F.S., Prezzi, M. & Salgad, R. 2014. Experimental study of cone penetration in silica sand using digital image correlation. Geotechnique, 64 (7), pp. 551-569.

Asaoka A., Noda, T. & Kaneda, K. 1998a. Displacement/traction boundary conditions represented by con-straint conditions on velocity field of soil. Soils and Foundations, 38 (4), pp. 173-181.

Asaoka, A., Nakano, M. & Noda, T. 1998b. Super loading yield surface concept for the saturated structured soils. Proc. 4th Eur. Conf. Num. Meth. Geotech. Engrg, NUMGE98, pp. 232-242.

Asaoka, A., Nakano, M. & Noda, T. 2000. Superloading yield surface concept for highly structured soil behav-ior, Soils and Foundations, 40 (2), pp. 99-110.

Asaoka, A., Noda, T., Yamada, E., Kaneda, K. & Nakano, M. 2002. An elasto-plastic description of two distinct vol-ume change mechanisms of soils. Soils and Foundations, 42 (5), pp. 47-57

Asaoka A. & Noda, T. 2007. All soils all states all round geo-analysis integration, International Workshop on Constitutive Modelling - Development, Implementation, Evaluation, and Application, Hong Kong, China, pp. 11-27.

Ma, H., Zhou, M., Hu, Y., & Hossain, S. M. 2017. Interpretation of Layer Boundaries and Shear Strengths for Stiff-Soft-Stiff Clays Using Cone Penetration Test: LDFE Analyses. Int. J. Geomechanics, 17(9), pp. 06017011-1-11, ASCE.

Mo, P.Q., Marshall, A.M. & Yu, H.S. 2015. Centrifuge modelling of cone penetration tests in layered soils. Geotechnique, 65 (6), pp. 468-481.

Mo, P.Q., Marshall, A.M. & Yu, H.S. 2017. Interpretation of Cone Penetration Test Data in Layered Soils Using Cavity Expansion Analysis, J. Geotech. Geoenviron. Eng., 143 (1), pp. 04016084-1-12.

Noda, T., Asaoka, A. & Nakano, M. 2008. Soil-water coupled finite deformation analysis based on a rate-type equation of motion incorporating the SYS Cam-clay model. Soils and Foundations, 48 (6), pp. 771-790.

Thevanayagam, Sl, Sivaratnarajah, U. & Huang, Q. 2017. Soil liquefaction screening using CPT - Effect of non-plastic silt content. Int. Symp, PBDIII, Paper #481.

Tolooiyan, A. & Gavin, K. 2011. Modelling the Cone Penetration Test in sand using Cavity Expansion and Arbitrary Lagrangian Eulerian Finite Element Methods. Computers and Geotechnics, 38 (4), pp. 482-490.